

# Dispersion control for matter waves and gap solitons in optical superlattices

Pearl J.Y. Louis, Elena A. Ostrovskaya, and Yuri S. Kivshar  
*Nonlinear Physics Centre and ARC Centre of Excellence for Quantum-Atom Optics,  
Research School of Physical Sciences and Engineering,  
The Australian National University, Canberra ACT 0200, Australia*

We present a numerical study of dispersion manipulation and formation of matter-wave gap solitons in a Bose-Einstein condensate trapped in an optical superlattice. We demonstrate a method for controlled generation of matter-wave gap solitons in a stationary lattice by using an interference pattern of two condensate wavepackets, which mimics the structure of the gap soliton near the edge of a spectral band. The efficiency of this method is compared with that of gap soliton generation in a moving lattice recently demonstrated experimentally by Eiermann *et al.* [Phys. Rev. Lett., **92**, 230401 (2004)]. We show that, by changing the relative depths of the superlattice wells, one can fine-tune the effective dispersion of the matter waves at the edges of the mini-gaps of the superlattice Bloch-wave spectrum and therefore effectively control both the peak density and the spatial width of the emerging gap solitons.

## I. INTRODUCTION

In recent years Bose-Einstein condensates (BECs) loaded into optical lattices have become an important tool in the studies of linear and nonlinear behavior of coherent waves in periodic systems. The band-gap structure of the matter-wave spectrum resulting from the periodicity of the optical trapping potential is responsible for much of the observed coherent behavior of the condensate, including Bloch oscillations and Landau-Zener tunnelling [1, 2]. One of the more dramatic effects of the lattice on the BEC dynamics is the dependence of the group-velocity dispersion of matter waves on the curvature of the spectral band. The latter, in turn, is a function of the wavepacket quasi-momentum in the lattice rest frame. Due to the possibility to create a moving optical lattice by varying the relative detuning of the interfering laser beams, the condensate can be loaded into the lattice with a well-defined quasi-momentum [3]. This enables precise engineering of the dispersion of the BEC wavepackets in moving optical lattices [4, 5].

Dispersion management of a BEC wavepacket loaded into a one-dimensional (1D) moving lattice was recently investigated experimentally [4, 5, 6], in both linear (non-interacting) and non-linear (weakly interacting) regimes. In the nonlinear regime, a balance between the effects of nonlinearity and dispersion can produce a *bright matter-wave soliton*, a localized BEC wavepacket that maintains a constant spatial structure. The creation of a bright soliton in a *repulsive* condensate (as opposed to an attractive condensate) is *only* possible due to the negative effective dispersion at the edge of the first Brillouin zone (BZ) of a 1D optical lattice (see e.g. [7]). Driving the condensate from the middle to the edge of the Brillouin zone achieves transition between the regimes of positive and negative effective dispersion. Evolution of the matter wavepacket in the negative dispersion regime can result in the self-focusing of the repulsive BEC in the form of a fundamental *gap soliton* [8].

The absolute value of the dispersion experienced by

a BEC wavepacket can be varied by changing the lattice depth [7, 8]. All previous studies on matter-wave dispersion management and gap solitons involved single-periodic *shallow* lattices [4, 5, 6, 8] which are characterized by narrow spectral gaps, greater curvatures of the spectral bands, and hence larger values of the effective dispersion at the gap edges. Stronger dispersion requires larger matter-wave nonlinearity, and hence larger atomic density, and/or wider wavepackets to achieve the localized state [8]. Therefore, dispersion manipulation in an optical lattice can potentially deliver control over the characteristics of BEC solitons.

In this paper, we explore novel possibilities to control the *magnitude* of dispersion experienced by a BEC wavepacket *at the edges of the spectral bands* by modifying the shape of a double-periodic optical *superlattice*. As known from the theory of diatomic lattices and semiconductor superlattices, an extra periodicity opens up additional narrow stop-gaps (or mini-gaps) in the band-gap spectrum. Here we show that the values of effective dispersion at the edges of these mini-gaps can be varied within a much greater range than it is possible for a single-period lattice of a reasonable depth.

To demonstrate the efficient dispersion control and generation of *immobile* gap solitons, we investigate the process of nonlinear localization in both moving and *stationary* superlattices. In the former case, in order to access the gap regions, the initially stationary condensate in the middle of the ground-state Brillouin zone is driven to the band edge by accelerating the lattice. By the end of the *adiabatic* acceleration process, the condensate wavepacket has a quasi-momentum and an internal structure of a linear Bloch wave at the gap edge. In this paper, we numerically simulate this process, starting from the initial adiabatic loading of the condensate into a quasi-1D superlattice. Our numerical simulations closely follow the current experimental procedure for matter-wave gap-soliton generation [8].

In addition, we suggest a new method for creating the correct initial conditions for the soliton formation at the gap edge in a *stationary* lattice, by interfering two identi-

cal wavepackets with equal momenta of the opposite sign, corresponding to the opposite edges of the first BZ. This enables us to efficiently create a matter wavepacket with the correct internal structure at the relevant gap edge and avoid large time scales associated with the adiabatic acceleration. Such a wavepacket preparation technique was previously explored in optics [9, 10, 11, 12, 13]. Here we show that this method leads to more efficient soliton generation and shape control of the emerging gap solitons via dispersion control in the superlattice.

## II. MATTER-WAVE SPECTRUM IN A SUPERLATTICE

In the mean-field approximation, the dynamics of a Bose-Einstein condensate is described by the Gross-Pitaevskii (GP) equation. Assuming that the condensate cloud is extremely elongated in the direction  $x$ , with the ratio of the corresponding frequencies  $\Omega = \omega_x/\omega_\perp \sim 0.1$  [5, 8, 14, 15], the condensate wavefunction in the axial dimension can be described by the one-dimensional (1D) GP equation (see, e.g., Ref. [16]):

$$i\frac{\partial\psi}{\partial t} = -\frac{1}{2}\frac{\partial^2\psi}{\partial x^2} + V(x,t)\psi + g_{1D}|\psi|^2\psi, \quad (1)$$

where  $V(x,t)$  is the external trapping potential, and  $g_{1D}$  characterizes the strength of the two-body interactions rescaled for the case of the 1D geometry. The structure of the condensate wavefunction in the transverse dimensions is determined by a tight harmonic potential.

Assuming that any additional trapping along the axial direction (e.g., due to a magnetic trap) is weak, we write  $V(x,t)$  as a periodic potential of a 1D optical superlattice:

$$V(x) = U[\varepsilon \sin^2(K_1x) + (1 - \varepsilon) \sin^2(K_2x)]. \quad (2)$$

The superlattice potential given by Eq. (2) can be obtained by superimposing two independent (either detuned from each other [15] or orthogonally polarized [17]) far off-resonance single-periodic standing waves with different periods  $d_1$  and  $d_2$ . The larger of the two periods, e.g.  $d = d_1$ , defines the coarse periodicity of the lattice. The lattice wavevectors are given by  $K_1 = \pi/d_1$  and  $K_2 = \pi/d_2$  where the commensurable periods are chosen such that  $d_1/d_2 = 2$ . The relative and total intensity of the standing waves are controlled by the parameters  $0 \leq \varepsilon \leq 1$  and  $U$  respectively.

Equation (1), with the lattice potential given by (2), was made dimensionless by using the characteristic length  $a_L = d/\pi$ , energy  $E_L = \hbar^2/ma_L^2 = 2E_{\text{rec}}$ , and time  $\omega_L^{-1} = \hbar/E_L$ , where  $m$  is the atomic mass. In these dimensionless units,  $g_{1D} = 2(a_s/a_L)(\omega_\perp/\omega_L)$ . Here we use the parameters of the  $^{87}\text{Rb}$  condensate:  $m = 1.44 \times 10^{-25}$  kg and  $a_s = 5.7$  nm. We assume that the periods of the standing waves forming the superlattice are  $d = d_1 = 350$  nm and  $d_2 = 175$  nm, so in the

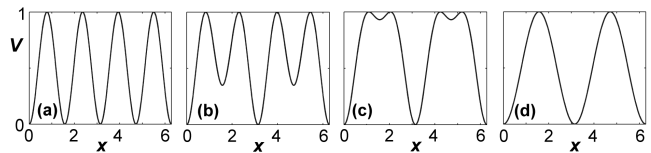


FIG. 1: The structure of the superlattice potential described by Eq. (2) for different values of  $\varepsilon$  and a fixed potential height  $V_0 = 1$ : single-periodic optical lattice for (a)  $\varepsilon = 0$  and (d)  $\varepsilon = 1$ , and double-periodic superlattices for (b)  $\varepsilon = 0.3$  and (c)  $\varepsilon = 0.7$ .

dimensionless units,  $K_1 = 1$  and  $K_2 = 2$ . With strong transverse confinement of  $\omega_\perp \sim 500 - 550\text{Hz}$  [8, 14, 18],  $g_{1D} \sim 0.001$ , and this is the value we use for most of the simulations in this paper.

The shape of the optical superlattice (2) depends on the values of the parameters,  $U$  and  $0 \leq \varepsilon \leq 1$ . In the limits  $\varepsilon \rightarrow 0$  or  $\varepsilon \rightarrow 1$ , the lattice becomes single-periodic, and  $U$  coincides with the height of the lattice  $V_0$ . For  $\varepsilon \neq 0$  and  $\varepsilon \neq 1$ , Eq. (2) describes a double-periodic superlattice with  $U$  defined through the amplitude of the periodic potential  $V_0$  as

$$U = 16V_0 \frac{(1 - \varepsilon)}{(4 - 3\varepsilon)^2}.$$

Figure 1 shows several examples of the superlattice potential (2) with the constant amplitude  $V_0 = 1$ . As seen in the figure, the relative depth of the large and small lattice wells can be manipulated by varying  $\varepsilon$ , whilst keeping the height of the lattice constant.

In the linear regime ( $g_{1D} = 0$ ), the stationary solutions to Eq. (1) with the periodic potential are Bloch waves:

$$\psi(x,t) = \phi(x)e^{-i\mu t} = u(x)e^{ik(\mu)x}e^{-i\mu t}, \quad (3)$$

where  $\mu$  is the matter-wave chemical potential and the function  $u(x)$  has the periodicity of the lattice. The linear matter-wave spectrum  $\mu(k)$  consists of bands where the real wavenumbers  $k(\mu)$  correspond to the oscillatory Bloch-wave solutions. The bands are separated by ‘‘gaps’’ where  $\text{Im}(k) \neq 0$ . Figure 2(a) shows the band-gap diagrams plotted in the extended zone scheme for a single-periodic lattice ( $\varepsilon = 0$ ) and a superlattice ( $\varepsilon = 0.05$ ), both for the lattice amplitude of  $V_0 = 5$ . Since the coarse periodicity of the superlattice is twice that of the single-periodic lattice, the size of the Brillouin zones of the superlattice are half that of the single-periodic lattice at  $\varepsilon = 0$ . This leads to mini-gaps appearing in the superlattice band-gap spectra at  $k = 1$ . A shaded stripe in Fig. 2(a) shows the lowest energy mini-gap at  $\varepsilon = 0.05$ . As  $\varepsilon$  grows, the size of the mini-gap increases.

For an interacting condensate ( $g_{1D} \neq 0$ ), the solutions of the model equation near the band (or mini-band) edges can be sought in the form:  $\psi(x,t) = \exp(-i\mu t)f(x,t)\phi(x)$ , where  $\phi(x)$  is the linear Bloch

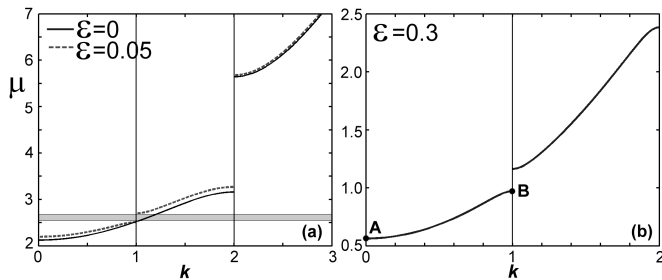


FIG. 2: (a) The band-gap spectra for a single-periodic optical lattice ( $\varepsilon = 0$ ) and a double-periodic superlattice with weak modulation ( $\varepsilon = 0.05$ ). In both cases, the lattice height is set to  $V_0 = 5$ . The first mini-gap is shaded. (b) The spectrum around the first mini-gap for a strongly modulated superlattice at  $V_0 = 1$  and  $\varepsilon = 0.3$ .

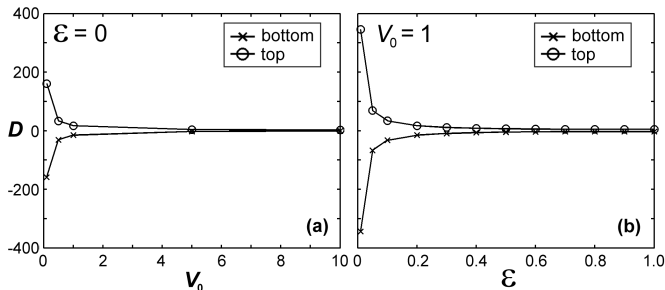


FIG. 3: The effective group-velocity dispersion  $D$  (a) at the edges of the first gap of a single-periodic optical lattice of varying strength, and (b) at the edges of the first mini-gap for a superlattice of height  $V_0 = 1$  and period  $d = \pi$ , as the shape of the superlattice is changed by varying  $\varepsilon$ .

wave at the corresponding band edge and  $f(x, t)$  is a slowly varying envelope [7, 19, 20]. Then, the dynamics of the envelope are governed by the reduced GP equation [7, 19, 20]:

$$i \frac{\partial f(x, t)}{\partial t} = \left\{ -\frac{D}{2} \frac{\partial^2}{\partial x^2} + \tilde{g}_{1D} |f(x, t)|^2 \right\} f(x, t), \quad (4)$$

where  $D = \partial^2 \mu / \partial k^2 = \partial v_g / \partial k$  is the effective group velocity ( $v_g$ ) dispersion and  $\tilde{g}_{1D} = g_{1D} \int |\phi(x)|^4 dx / \int |\phi(x)|^2 dx$ .

Figure 3(a) shows the effective group velocity dispersion,  $D$ , near the lowest energy gap of a single-period lattice for varying lattice height. As seen in Fig. 3(a), the dispersion is negative at the bottom of the gap and positive at the top. As the condition  $g_{1D} D < 0$  is required for the formation of bright gap solitons, bright gap soliton families originate near the bottom of the gaps, for repulsive condensates ( $g_{1D} > 0$ ), and near the top of the gaps, for attractive condensates ( $g_{1D} < 0$ ) [21, 22, 23, 24], and exist for the entire range of chemical potentials within that gap. The group velocity  $v_g = \partial \mu / \partial k$  vanishes at

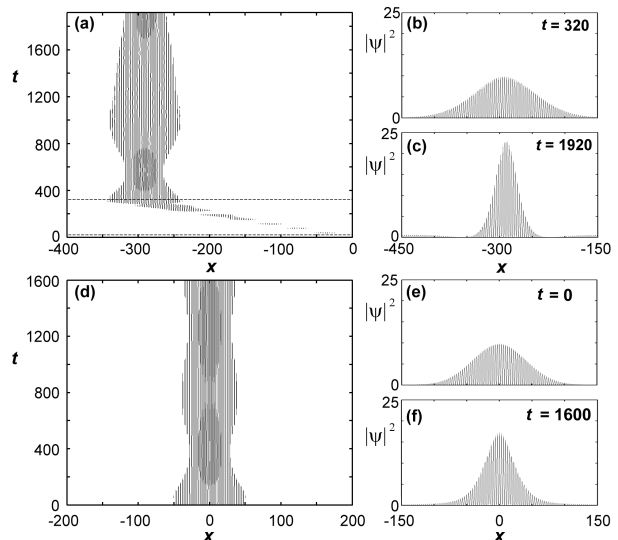


FIG. 4: Soliton generation by (a) a single Gaussian wavepacket accelerated to the edge of the first mini-gap ( $k = 1$ ) in a moving superlattice and (d) interference of two counter-propagating Gaussian wavepackets in a stationary superlattice. Both superlattices have  $\varepsilon = 0.3$  and  $V_0 = 1$ . Figure (a) is plotted in the lattice frame moving at  $v_{rec}$ . Initially the wavepacket contains 500 atoms, and has a width parameter of  $w = 100$ . In (d) the initial parameters are  $w = 81.6$  and  $N = 500$ . (b,c) and (e,f) capture the spatial structure of the wavepackets at different evolution times.

the band edges, hence the gap solitons form as immobile localized wavepackets.

Gap soliton formation can also occur in the minigaps of the superlattice spectrum. The size of the mini-gap increases with growing  $\varepsilon$ . This decreases the curvature in the band structure immediately surrounding the mini-gap, leading to a decrease in the magnitude of the effective dispersion at the gap edges. Figure 3(b) shows that simple variation of the relative depths of the two wells in the superlattice (i.e.  $\varepsilon$ ) at a constant lattice height ( $V_0 = 1$ ) opens up access to a large range of effective dispersions at the edges of the mini-gap. As Figure 3(a) shows, this kind of dispersion control can also be performed in a single-periodic lattice by changing the lattice height. However, the range of effective dispersion values in a single-periodic lattice is much smaller than that achievable in a superlattice, and the larger proportion of this range is only accessible for  $V_0 < 1$ .

### III. GAP-SOLITON GENERATION IN A MOVING LATTICE

The key to producing a spatial gap soliton in a BEC is to access the band-gap edge of the linear spectrum, where the suitable effective dispersion can assist spatial

self-focusing of the coherent matter waves. For a repulsive condensate, this occurs at the bottom edge of the first gap, where the dispersion is negative. In experiments, the stationary condensate is initially loaded into the lattice ground state by slowly ramping up the lattice height. This produces a wavepacket in the lowest energy band ( $n = 0$ ) in the middle of the first Brillouin zone (centered at  $k = 0$ ). To ensure that other energy bands are not populated, the ramping process should be adiabatic. To adiabatically load the condensate into the lattice at quasi-momentum  $k$ , the change of the single-particle BEC Hamiltonian on the time scale of a single Rabi oscillation associated with the transition between the Bloch states in the ground state,  $\phi_{0,k}$ , and the first excited band,  $\phi_{1,k}$ , should be much smaller than the energy gap between the  $n = 0$  and  $n = 1$  bands at quasi-momentum  $k$ . In our dimensionless units, this adiabaticity condition translates to  $\Delta V_0/t_R \ll \Delta\mu^2(k)$  ([3, 25, 26]), where  $t_R$  is the duration of the lattice ramp-up,  $\Delta V_0$  is the total change of the lattice amplitude, and  $\Delta\mu(k)$  is the size of the first (mini)gap at the quasi-momentum  $k$ . In the middle of the Brillouin zone (BZ), at  $k = 0$ , the size of the first mini-gap is equal to four single-photon recoil energies [3]. Therefore, the single-particle adiabaticity condition for loading a stationary condensate into the lattice at  $k = 0$  is,  $\Delta V_0/t_R \ll \Delta\mu^2(k = 0) = 4$ .

In order to access the band edge, a constant acceleration is introduced *suddenly* [3], by applying time-dependent frequency detuning to the lasers used to create the lattice. The superlattice potential given by Eq.(2) becomes time-dependent:  $V(x, t) = U[\varepsilon \sin^2(K_1(x - \delta t)) + (1 - \varepsilon) \sin^2(K_2(x - \delta t))]$ . Then, the reference frame in which the lattice is stationary (the lattice rest frame) is moving in the laboratory frame with velocity  $v(t) = \delta(t)$ . If the acceleration,  $a = d\delta/dt$ , is constant, a constant and uniform force is applied to the condensate [25], which is somewhat analogous to the application of a constant homogeneous electric field to electrons in a crystal. The quasi-momentum of the condensate depends on the duration of the acceleration,  $t_A$ , as  $k(t_A) = k(0) + at_A$ , and in order to move the condensate to the band-edge ( $k(t_A) = 1$ ), the recoil velocity  $v_{\text{rec}} = 1$  of the lattice is reached with acceleration  $a = 1/t_A$ . The acceleration is adiabatic, i.e. the upper bands are not populated, provided the probability of transitions between the  $n = 0$  and  $n = 1$  bands are low. This requires a small magnitude of the acceleration,  $|\Delta\delta/t_A| \ll \Delta\mu(k)$  [25]. For acceleration at a constant lattice height, the critical energy gap is at the edge of the Brillouin zone ( $k = \pm 1$ ), where the gap is generally much smaller than that at  $k = 0$ , as can be seen in Fig. 2. The ramping adiabaticity condition is also much harder to fulfil at the band-gap edge than in the middle of the Brillouin zone. This is why it is preferable to load the condensate into the lattice at  $k = 0$  and then accelerate it to the band-edge instead of simply ramping up an already moving lattice at velocity  $v_{\text{rec}}$ .

We model the process of ramping and accelerating the lattice by starting with an initially stationary Gaussian wavepacket:  $\psi(x, t = 0) = A \exp(-x^2/w^2)$  where  $A$  is the amplitude and  $w$  is the width. Figure 4(a) shows the three stages of the evolution of an initially Gaussian wavepacket with  $w = 100$  and  $N = 500$  atoms in a superlattice with  $\varepsilon = 0.3$  and a potential depth of  $V_0 = 1$  [the band-gap structure of this lattice is shown in Fig. 2(b)]:

- The superlattice is ramped up from  $V_0 = 0$  to  $V_0 = 1$  in time  $t_R = 20$ . This places the wavepacket at  $k = 0$  in the lowest energy band [point A in Fig. 2(b)]. The wavepacket develops an internal structure with the same spatial properties as a Bloch wave at  $k = 0$ .
- The superlattice is accelerated to the edge of the first mini-gap [point B in Fig. 2(b)] in time  $t_A = 300$ .
- The wavepacket is then left to evolve in a superlattice moving with constant velocity  $v_{\text{rec}}$  i.e. at the edge of the Brillouin zone. Figures 4(a-c) are plotted in a frame moving at the recoil velocity  $v_{\text{rec}}$  so that the wavepacket appears stationary when it is at the gap edge where its group velocity with respect to the lattice is zero.

For sufficiently long times of the wavepacket evolution at the mini-band edge, a localized wavepacket with the spatial structure of a gap soliton emerges, as seen in Fig. 4(c). A fundamental gap soliton near a gap edge takes the form of a broad sech-shaped envelope with an internal structure resembling the linear Bloch waves at that particular edge. This spatial structure allows sufficiently broad gap solitons to be described using a wave-envelope approximation with an appropriately chosen carrier wave, as described in the previous section. Due to large differences between the ideal shape of the soliton and the shape of the initial wavepacket, significant oscillations in the shape of the wavepacket are observed [see Fig. 4(a)]. This is also a well known part of soliton formation in the absence of the lattice [27, 28]. The closer the initial width of the wavepacket is to that of the soliton, the more efficient is the process of soliton generation. This is illustrated in Figs. 4(d-f), where a slightly narrower initial wavepacket was used. As a general guide, the peak density and width of the initial wavepacket required for the formation of the fundamental gap soliton are related as:  $A^2 \sim |D|/(w^2\tilde{g}_{1D})$  (see [27], ch. 5). While the time scale in Figs. 4(a,d) is not sufficient to see the shape of the wavepacket stabilize, as we evolve the wavepacket even further, it is clear that the oscillations are gradually being damped as excess atoms are removed into the low-density background.

The spatial extent of the initial wavepacket is required to be large ( $\sim 90$  lattice sites), so that the momentum distribution is very narrow compared to the size of the Brillouin zone. The acceleration process works

best with a narrow momentum distribution and hence a wide wavepacket, which is broader than the soliton that is eventually formed. If the momentum distribution is too broad, undesirable effects may occur, e.g. the wavepacket can develop a strong asymmetry as it passes through the zero dispersion point, as described in Ref. [4]. A wide initial wavepacket also reduces the maximum density in the initial wavepacket used to form a fundamental soliton since the width of the fundamental soliton's envelope near the band edge is inversely proportional to its amplitude,  $A \sim 1/w$  [27].

For both the ramping and acceleration processes, we have checked the momentum components of the wavepacket to ensure that there is no significant excitation of the upper bands. As discussed above, the rate at which the lattice can be adiabatically accelerated depends very strongly on the size of the energy gap. The size of the mini-gaps for superlattices with  $\varepsilon \ll 1$  are much smaller than the size of the gaps of a single-periodic lattice for the same lattice height. This makes the above described techniques for condensate preparation at the edges of a superlattice mini-gap rather difficult to use due to the large acceleration times.

Difficulty in accelerating the condensate to the gap edge for narrow gaps produced in shallow single-periodic optical lattices was also noted in recent experiments [8]. However, smaller gaps are useful because they potentially enable greater values of the effective dispersion [see Fig. 3(a)]. Below, we study an alternative scheme for gap-soliton generation in a *stationary* lattice. Since the problems of large time-scales associated with conditions of adiabatic ramping and acceleration are avoided in this case, the method would be equally useful for low modulation height single-periodic optical lattices and superlattices with narrow mini-gaps.

#### IV. GAP-SOLITON GENERATION IN A STATIONARY LATTICE

An alternative method for creating a wavepacket with the correct quasi-momentum and internal structure to produce *spatial gap solitons* was first suggested theoretically in the context of nonlinear optics [9, 10, 11], and was recently employed in experiments on weakly coupled waveguide arrays and optically-induced photonic lattices [12, 13]. Applied to matter waves in optical lattices, this technique means that, instead of using a moving lattice to gradually drag a BEC wavepacket to the edge of the Brillouin zone, we start with two non-stationary wavepackets with opposite momenta (i.e.  $k = 1$  and  $k = -1$ ) corresponding to the Bragg reflection condition in a *stationary* lattice. Their interference produces a matter wave with the internal structure resembling that of the Bloch wave at the gap edge. This is expected since the Bloch wave at the edge of a gap is a periodic standing wave formed at the Bragg reflection condition and hence can be presented as the superposition of identical for-

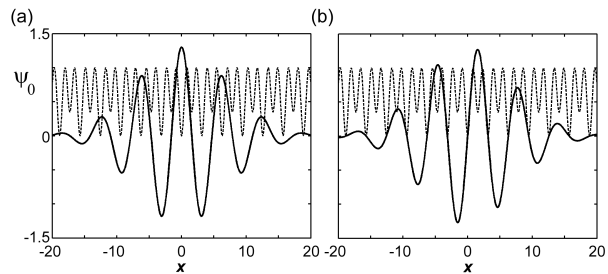


FIG. 5: Interference patterns of two Gaussian wavepackets as described by Eq. (5) with  $A = 1.3$ ,  $k = 1$ ,  $w = 10$ , and (a)  $\theta_1 = 0$ ,  $\theta_2 = 0$ , and (b)  $\theta_1 = 3\pi/2$ ,  $\theta_2 = \pi/2$ . Dotted lines show the superlattice potential ( $\varepsilon = 0.3$  and  $V_0 = 1$ ).

ward and backward moving travelling waves. Recently this method was used to theoretically demonstrate the formation of optical spatial gap solitons in binary waveguide arrays, the nonlinear optical analogue to our particular optical superlattice system [11] for a focusing (attractive) nonlinearity. In Ref. [11] it was found that this method allows for the efficient production of spatial gap solitons at the top of the mini-gap. Here we apply this method to *repulsive* condensates (and hence the soliton formation at the *bottom* of the mini-gap).

We assume the initial state of condensate evolution in the form of two identical Gaussian wavepackets,  $\psi_1(x, t = 0)$  and  $\psi_2(x, t = 0)$ , with momenta  $k_1 = k$  and  $k_2 = -k$  and phases  $\theta_1$  and  $\theta_2$  respectively. These wavepackets could be created using Bragg scattering techniques. Assuming that both wavepackets are initially centered at the origin, their superposition is given by the expression:

$$\psi(x, t = 0) = Ae^{-x^2/w^2} [e^{ikx+i\theta_1} + e^{-ikx+i\theta_2}], \quad (5)$$

where  $A$  is a constant amplitude and  $w$  is a width. By setting the correct  $k$ ,  $\theta_1$  and  $\theta_2$ , the symmetry of  $\psi(x, t = 0)$  can be matched to that of the Bloch waves at various gap edges. For example, with  $k = 1$ ,  $\theta_1 = \theta_2 = 0$ , Eq. (5) simplifies to  $\psi(x, t = 0) = A \exp(-x^2/w^2) \cos(x)$ , which has the spatial structure of the Bloch wave at the bottom edge of the first mini-gap of a superlattice potential [see, e.g., Fig. 5(a)]. Setting  $k = 1$ ,  $\theta_1 = 3\pi/2$ , and  $\theta_2 = \pi/2$  gives  $\psi(x, t = 0) = -A \exp(-x^2/w^2) \sin(x)$  which mimics the Bloch wave at the top edge of the first mini-gap [see, e.g., Fig. 5(b)].

In what follows we study the generation of matter-wave gap solitons in the two cases discussed above. That is, (a)  $k = 1$ ,  $\theta_1 = 0$  and  $\theta_2 = 0$  i.e. at the bottom of the first superlattice mini-gap and (b)  $k = 1$ ,  $\theta_1 = 3\pi/2$  and  $\theta_2 = \pi/2$  i.e. at the top of the first superlattice mini-gap. We consider wavepackets containing  $N = 1000$  atoms, with the width of the spatial envelope set at  $w = 30$  which means the initial wavepacket occupies around 30 wells. With this soliton excitation method, we can use wavepackets with small widths that are closer to the fun-

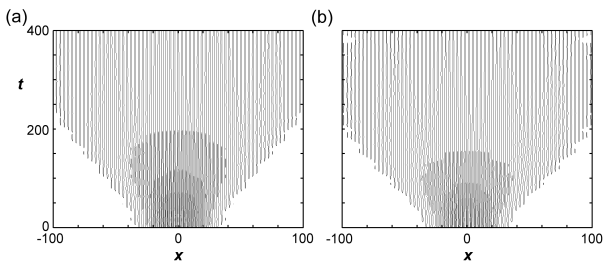


FIG. 6: Linear ( $g_{1D} = 0$ ) evolution of wavepackets formed by the interference of two Gaussian wavepackets described by Eq. (5) in a superlattice potential ( $\varepsilon = 0.3$  and  $V_0 = 1$ ). Number of atoms is  $N = 1000$ ,  $k = 1$ , and  $w = 30$ . In (a) the phases of the two wavepackets are  $\theta_1 = 0$  and  $\theta_2 = 0$ . In (b) the phases are  $\theta_1 = 3\pi/2$  and  $\theta_2 = \pi/2$ , respectively.

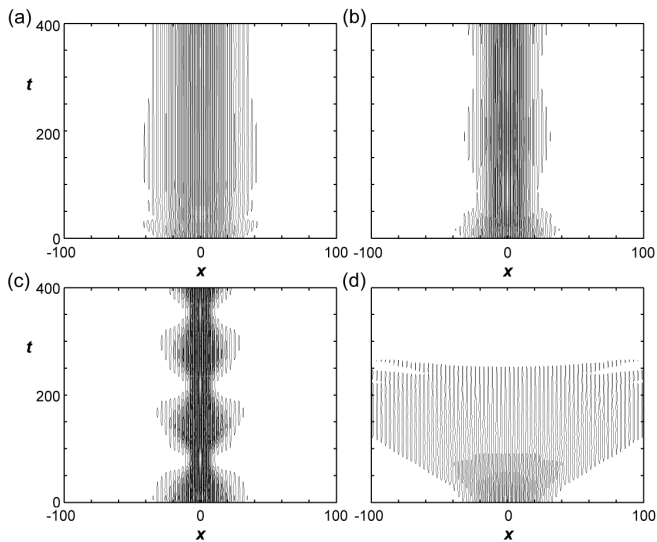


FIG. 7: Evolution of wavepackets described by Eq. (5) with repulsive interaction  $g_{1D} = 0.001$ ,  $N = 1000$ ,  $k = 1$ , and  $w = 30$ . In (a)-(c)  $\theta_1 = 0$  and  $\theta_2 = 0$  i.e. the wavepacket is at the bottom of the first mini-gap. In (d)  $\theta_1 = 3\pi/2$  and  $\theta_2 = \pi/2$  i.e. the wavepacket is at the top of the first mini-gap. Each of the superlattice potentials have the same period and lattice height  $V_0 = 1$ . The shape of each superlattice however varies: (a)  $\varepsilon = 0.2$ , (b) and (d)  $\varepsilon = 0.3$ , (c)  $\varepsilon = 0.5$ .

damental soliton width at the corresponding atom number, as a small initial momentum distribution is not crucial. If the initial wavepacket has a smaller width, then we can use a larger nonlinearity, i.e. larger peak density, and still obtain a fundamental soliton [27]. Using Eq. (5) as the initial condition, we solve the 1D evolution equation (1) with the stationary superlattice potential (2), by employing a Fourier split-step method implemented using the code generator XMDS [29]

In the absence of nonlinearity ( $g_{1D} = 0$ ), we expect

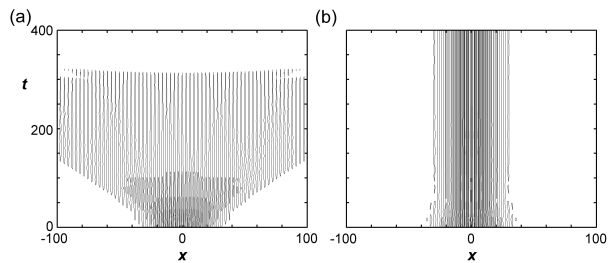


FIG. 8: Evolution of a wavepacket formed by the interference of two Gaussian wavepackets as described by Eq. (5) in a superlattice potential with  $V_0 = 1$  and  $\varepsilon = 0.3$  for  $N = 1000$ ,  $k = 1$ , and  $w = 30$ . In contrast to Figs. 7(b) and (d), we use an attractive nonlinearity,  $g_{1D} = -0.001$ . In (a)  $\theta_1 = 0$  and  $\theta_2 = 0$  i.e. the wavepacket is at the bottom the first mini-gap. In (b)  $\theta_1 = 3\pi/2$  and  $\theta_2 = \pi/2$  so that the wavepacket is at the top of the first mini-gap.

that the initial wavepacket disperses and spreads out. Figure 6 shows this occurring for both cases (a) and (b) in a superlattice with  $\varepsilon = 0.3$  and  $V_0 = 1$ . The wavepacket at the top of the mini-gap [Fig. 6(b)] exhibits slightly greater dispersion than the wavepacket at the bottom of the mini-gap [Fig. 6(a)], which agrees with the values of the effective dispersion coefficient shown in Fig. 3.

When a repulsive nonlinearity ( $g_{1D} > 0$ ) is "turned on", the interplay between negative dispersion and positive nonlinearity ( $g_{1D}D < 0$ ) results in the localization of the initial wavepacket into a gap soliton at the bottom of the mini-gap [see Figs. 7(a-c)]. In contrast, at the top of the mini-gap the repulsive nonlinearity interacts with the positive dispersion ( $g_{1D}D > 0$ ) to accelerate the spreading and breakup of the BEC wavepacket [see Fig. 7(d)]. When an attractive nonlinearity ( $g_{1D} < 0$ ) is used instead, the wavepacket forms a gap soliton at the top of the mini-gap while the one at the bottom breaks up more quickly [see Fig. 8]. In the three cases shown in Figs. 7(a-c), the fraction of atoms radiated from the wavepacket during the process of gap-soliton formation is less than 10%. In addition, the localization occurs over time intervals that are almost an order of magnitude shorter than those for the transient dynamics of the wavepackets in the moving lattices.

In general, the interference method of gap-soliton generation allows for more precise control of the initial wavepacket widths, uninhibited by any requirements on the initial momentum distribution. This allows us to perform an accurate analysis of the effects of dispersion on the BEC localization process in the superlattice potential by creating an initial wavepacket at the band-gap edge with exactly the same parameters for each superlattice. The effects of the dispersion control are demonstrated in Figs. 7(a-c), which show the gap-soliton generation in a mini-gap for three different shapes of the superlattice potentials and the same repulsive nonlinearity ( $g_{1D} = 0.001$ ). In each case, the lattice period and

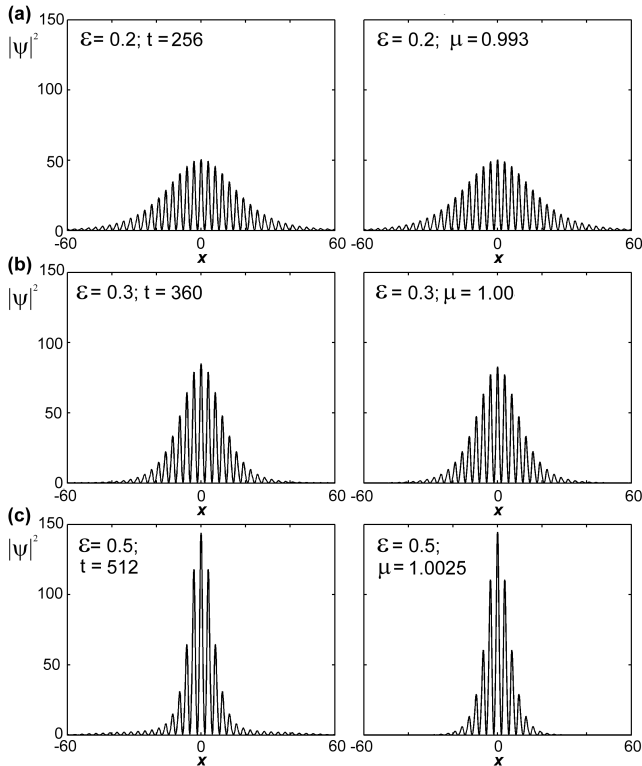


FIG. 9: Left: Density profiles of the pulses shown in Figures 7(a)-(c). The initial conditions are identical in each case, but the superlattice potential varies with (a)  $\varepsilon = 0.2$ , (b)  $\varepsilon = 0.3$  and (c)  $\varepsilon = 0.5$ . In each case the lattice height is  $V_0 = 1$ . Right: Stationary fundamental soliton solutions obtained by numerically solving the time-independent GP equation for the same superlattice parameters as on the left.

height are kept constant, as are the parameters of the initial wavepacket. The superlattice parameter  $\varepsilon$  varies and with it the relative well-depths of the small and large wells in the superlattice potential. With growing  $\varepsilon$ , the generated gap soliton becomes narrower and the average peak density increases. The dramatic change in the shape of the output soliton with variations in  $\varepsilon$  is due to the variations in the effective dispersion with  $\varepsilon$ , as seen in Fig. 3(b).

Figure 3 shows that as  $\varepsilon \rightarrow 1$  the magnitude of the effective dispersion at the edges of the superlattice band-gap decreases due to the increasing size of the mini-gap.

Consequently, the peak particle density required to form a soliton with the *same number of atoms* needs to increase to compensate. In Fig. 9 we show the density profiles of the pulses shown in Figs. 7(a-c) compared with the *stationary* fundamental soliton solutions obtained numerically by solving the time-independent GP equation for identical superlattice parameters. Because of the transient oscillations in the peak density of the dynamically generated gap solitons, we use the average value over time for this comparison. In each case, the matter-wave chemical potential is around the value  $\mu = 1.0$ , which is close to the bottom edge of the mini-gap for each of the three values of  $\varepsilon$ .

## V. CONCLUSIONS

In this paper, we have investigated an effective method of generating matter-wave gap solitons - nonlinear localized states of a repulsive Bose-Einstein condensate in a *stationary* optical lattice. We demonstrated that, by interfering two matter waves, one can create a wavepacket located at the gap edge with the appropriate internal structure suitable for gap soliton formation. The initial wavepacket prepared in this fashion can be better matched to the shape of the fundamental gap soliton, which leads to a more efficient and faster soliton formation compared to the standard technique of lattice acceleration. This method would be especially useful for small energy gaps, e.g. in the case of superlattice mini-gaps and for extremely shallow single-periodic optical lattices, where preparation of the condensate wavepackets at a gap edge by using lattice acceleration is experimentally difficult and time consuming. Using the interference method to simulate the gap soliton formation in double-periodic optical superlattices, we have shown that it is possible to fine-tune the effective dispersion of matter waves by changing the shape of the superlattice rather than its height or periodicity, and hence tailor the properties of the BEC solitons.

## VI. ACKNOWLEDGEMENTS

This work has been supported by the Australian Research Council (ARC). The authors thank Andrey Sukhorukov, Markus Oberthaler, Dmitry Pelinovsky, and Dmitry Skryabin for useful discussions and suggestions.

- 
- [1] M. Cristiani, O. Morsch, J. H. Müller, D. Ciampini, and E. Arimondo, Phys. Rev. A **65**, 063612 (2002).
  - [2] M. Jona-Lasinio, O. Morsch, M. Cristiani, N. Malossi, J. H. Müller, E. Courtade, M. Anderlini, and E. Arimondo, Phys. Rev. Lett. **91**, 230406 (2003).
  - [3] J. H. Denschlag, J. E. Simsarian, H. Häffner, C. McKen-

- zie, A. Browaeys, D. Cho, K. Helmerson, S. L. Rolston, and W. D. Phillips, J. Phys. B **35**, 3095 (2002).
- [4] B. Eiermann, P. Treutlein, Th. Anker, M. Albiez, M. Taglieber, K.-P. Marzlin, and M. K. Oberthaler, Phys. Rev. Lett. **91**, 060402 (2003).
- [5] L. Fallani, F. S. Cataliotti, J. Catani, C. Fort, M. Mod-

- ugno, M. Zawada, and M. Inguscio, Phys. Rev. Lett. **91**, 240405 (2003).
- [6] Th. Anker, M. Albiez, B. Eiermann, M. Taglieber, and M. K. Oberthaler, Opt. Express **12**, 11 (2004).
- [7] H. Pu, L. O. Baksmaty, W. Zhang, N. P. Bigelow, and P. Meystre, Phys. Rev. A **67**, 043605 (2003).
- [8] B. Eiermann, Th. Anker, M. Albiez, M. Taglieber, P. Treutlein, K.-P. Marzlin, and M. K. Oberthaler, Phys. Rev. Lett. **92**, 230401 (2004).
- [9] J. Feng, Opt. Lett. **18**, 1302 (1993).
- [10] A. V. Yulin, D. V. Skryabin, and W. J. Firth, Phys. Rev. E **66**, 046603 (2002).
- [11] A. A. Sukhorukov and Yu S. Kivshar, Opt. Lett. **28**, 2345 (2003).
- [12] D. Mandelik, R. Morandotti, J. S. Aitchison, and Y. Silberberg, Phys. Rev. Lett. **92**, 093904 (2004).
- [13] D. Neshev, A. A. Sukhorukov, B. Hanna, W. Krolikowski, and Yu. S. Kivshar (2004), nlin.PS/0311059.
- [14] S. Burger, F. S. Cataliotti, C. Fort, F. Minardi, M. Inguscio, M. L. Chiofalo, and M. P. Tosi, Phys. Rev. Lett. **86**, 4447 (2001).
- [15] S. Peil, J. V. Porto, B. L. Tolra, J. M. Obrecht, B. E. King, M. Subbotin, S. L. Rolston, and W. D. Phillips, Phys. Rev. A **67**, 051603 (2003).
- [16] A. D. Jackson, G. M. Kavoulakis, and C. J. Pethick, Phys. Rev. A **58**, 2417 (1998).
- [17] G. Grynberg and C. Robilliard, Phys. Rep. **355**, 335 (2001).
- [18] C. Fort, F. S. Cataliotti, L. Fallani, F. Ferlaino, P. Maddaloni, and M. Inguscio, Phys. Rev. Lett. **90**, 140405 (2003).
- [19] C. M. de Sterke and J. E. Sipe, Phys. Rev. A **38**, 5149 (1988).
- [20] M. J. Steel and W. P. Zhang (1998), cond-mat/9810284.
- [21] O. Zobay, S. Pötting, P. Meystre, and E. M. Wright, Phys. Rev. A **59**, 643 (1999).
- [22] P. J. Y. Louis, E. A. Ostrovskaya, C. M. Savage, and Yu. S. Kivshar, Phys. Rev. A **67**, 013602 (2003).
- [23] N. K. Efremidis and D. N. Christodoulides, Phys. Rev. A **67**, 063608 (2003).
- [24] D. E. Pelinovsky, A. A. Sukhorukov, and Yu. S. Kivshar, arXiv:nlin.PS/0405019.
- [25] E. Peik, M. Ben Dahan, I. Bouchoule, Y. Castin, and C. Salomon, Phys. Rev. A **55**, 2989 (1997).
- [26] A. M. Dudarev, R. B. Diener, and Q. Niu, J. Opt. B **6**, S231 (2004).
- [27] G. P. Agrawal, *Nonlinear Fiber Optics* (Academic Press, San Diego, 2001), 3rd ed.
- [28] D. Burak and W. Nasalski, Appl. Opt **33**, 6393 (1994).
- [29] The xmnds website is at <http://www.xmnds.org>.